Design of atomic ordering in $Mo_2Nb_2C_3T_x$ MXenes for hydrogen evolution electrocatalysis

Brian C. Wyatt [1], Anupma Thakur [1], Kat Nykiel [2], Zachary D. Hood [3], Shiba P. Adhikari [3], Krista K. Pulley [1], Wyatt J. Highland [1], Alejandro Strachan [2,*], Babak Anasori [1,2,*]

[1] – Department of Mechanical & Energy Engineering and Integrated Nanosystems Development Institute, Purdue School of Engineering & Technology, Indiana University – Purdue University Indianapolis, Indianapolis, IN 46202, USA
[2] - School of Materials Engineering and Birck Nanotechnology Center, Purdue University, West Lafayette, IN 47907, USA
[3] - Applied Materials Division, Argonne National Laboratory, Lemont, IL 60439, USA
[*] - Corresponding authors. Alejandro Strachan: strachan@purdue.edu. Babak Anasori: banasori@iupui.edu

Abstract (150 words):

The need for novel materials for energy storage and generation calls for chemical control at the atomic scale in nanomaterials. Ordered double transition metal MXenes expanded the chemical diversity of the family of atomically layered 2D materials since their discovery in 2015. However, atomistic tunability of ordered MXenes to achieve ideal composition-property relationships has not been yet possible. In this study, we demonstrate the synthesis of $Mo_{2+\alpha}Nb_{2-\alpha}AlC_3$ MAX phases ($0 \leq \alpha \leq 0.3$) and confirm the preferential ordering behavior of Mo and Nb in the outer and inner M layers, respectively, using density functional theory, Rietveld refinement, and electron microscopy methods. We also synthesize their 2D derivative $Mo_{2+\alpha}Nb_{2-\alpha}C_3T_x$ MXenes and exemplify the effect of preferential ordering on its hydrogen evolution reaction electrocatalytic behavior. This study seeks to inspire further exploration of the ordered double-transition metal MXene family and contribute composition-behavior tools toward application-driven design of 2D materials.

Keywords: MXene, o-MXene, 2D materials, tunable performance, hydrogen evolution reaction, electrocatalysis

Main Text (3000 words, excluding figures, figure description, references):

Two-dimensional (2D) layered materials provide unique and highly useful avenues for structural and composition-based design of active nanomaterials for electrochemical and catalytic processes.[1-5] Since their discovery in 2011, the number of reported synthesized compositions of 2D layered MXenes has expanded past 40 compositions.[6] MXenes are layered 2D materials denoted by their chemical notation $M_{n+1}X_nT_x$ ($1 < n < 4$), where M stands for n+1 layers of one or more 3*d*-5*d* block transition metals of groups 3-6 of the periodic table, X stands for n layers of carbon or nitrogen, and T_x stands for surface-bonded groups, commonly –O, –F, –Cl, or –(OH).[7, 8]

First discovered in 2015, out-of-plane ordered double transition metal MXenes, also known as o-MXenes, have gained increasing interest within the 2D community.[9, 10] In the traditional hexagonal lattice structure of $M_3C_2T_x$ and $M_4C_3T_x$ MXenes, the two transition metals in MXenes can either occupy random sites amongst all M layers, referred to as solid solution MXenes (such as, $(Mo_{1-\gamma}V_\gamma)_4AlC_3$),[11, 12] or in distinct separate M layers, referred to as out-of-plane ordered MXenes (o-MXenes, such as $Mo_2Ti_2C_3T_x$, as shown in Figure 1a).[9, 10, 13] However, there has been no possibility of further tunability of the M layer ordering and compositions for desired properties despite a few synthesized compositions and over 20 predicted yet unrealized phases of o-MXenes.[9, 10, 13-16]

In this study, we report on a set of an ordered molybdenum-niobium double transition metal carbide $Mo_{2+\alpha}Nb_{2-\alpha}C_3T_x$ o-MXene and present evidence for and the effect of partial substitution of the Nb atoms with Mo (α) in the inner atomic planes on the hydrogen evolution reactions (HER) as shown schematically in Figure 1b. Overall, this study indicates that ordered double transition metal MXenes have potential for atomic-level tuning for next-generation energy conversion devices (such as HER shown in Figure 1c).

Figure 1. Application-driven control of ordered double transition metal $Mo_{2+\alpha}Nb_{2-\alpha}C_3T_x$ provides control over the electrocatalytic HER behavior of MXenes. (a) Ordering in previous $Mo_2Ti_2C_3T_x$ MXenes is fixed, where transition metals are segregated into separate M atomic layers. (b) $Mo_{2+\alpha}Nb_{2-\alpha}C_3T_x$ MXenes allow controllable ordering in the M layers. (c) The gained control in $Mo_{2+\alpha}Nb_{2-\alpha}C_3T_x$ MXenes permits designable material behavior, as demonstrated in hydrogen evolution reaction catalytic applications.

We focused on this composition as Mo-Nb MXenes have been predicted stable when Mo atoms occupy the outer M layers (M') and Nb atoms occupy the inner M layers (M'') in a M_4C_3 structure in a Mo-C-Nb-C-Nb-C-Mo arrangement (Figure 1b).[10, 14] To investigate these predictions, we mixed elemental molar ratios of Mo:Nb from Mo-rich to Nb-rich with Mo:Nb:Al:C ratios ranging from 0.7:3.3:1.1:2.7 to 3.2:0.8:1.1:2.7 (Figure S1), where Al and C were kept in molar ratios consistent with the synthesis of similar M_4AlC_3 systems (See supplementary information).[11] Investigation of the full range of Mo:Nb molar ratios was essential to determine compositions which form stable M_4AlC_3 systems and determine their ordering. After mixing, we sintered these powder mixtures at 1600 °C for 4 h under argon flow of ~100 mL/min,[17] as shown in Figure 2a.

We used x-ray diffraction (XRD) to determine which phases indicated the presence of a M_4AlC_3 MAX phase and measure their *c*-lattice parameters. Figures 2b and S1 illustrate that clear M_4AlC_3 MAX phases were obtained *only* when two or more moles of Mo are used in the starting powder mixture, the first indication of atomic ordering.[18] Figure 2c demonstrates that the (002) and (004) peaks of the M_4AlC_3 MAX phases change only slightly in position/intensity depending on the composition, which is the second indication of ordering. Across all mixtures of Mo:Nb:Al:C used to synthesize M_4AlC_3 phases, we only observed a change of ±0.06Å in *c*-LP (Table S1). This small change in *c*-LP for our Mo:Nb:Al:C based M_4AlC_3 is in contrast with solid solutions M_4AlC_3 structures, such as $(Mo_{1-\gamma}V_\gamma)_4AlC_3$, which exhibit a ±0.10Å *c*-LP difference across 1:3:1.1:2.7 to 2:2:1.1:2.7 for Mo:V:Al:C.[11] We would expect the changes in *c*-LPs in a supposed solid solution $(Mo_{1-\gamma}Nb_\gamma)_4AlC_3$ should be larger than $(Mo_{1-\gamma}V_\gamma)_4AlC_3$, as the covalent radii difference is larger for Mo-Nb and Mo-V (9 pm and 4 pm, respectively),[19] which was not observed.

Figure 2. Synthesis of a M_4AlC_3 MAX phase obtained by mixing Mo:Nb:Al:C ratios of 1.8:2.2:1.3:2.7 to 3.2:0.8:1.3:2.7. (a) Schematic of inert pressureless sintering of Mo:Nb:Al:C powder mixtures. (b) Full-pattern x-ray diffraction data of obtained M_4AlC_3 MAX powders from the sintered Mo:Nb:Al:C mixtures. (c) Focus on the (002) and (004) peaks of the obtained M_4AlC_3 powders from the sintered Mo:Nb:Al:C mixtures. (d) Energy dispersive x-ray spectroscopy mapping for Mo and Nb content in the M_4AlC_3 grains across Mo:Nb:Al:C ratios.

After identifying the synthesis of Mo, Nb, Al, and C containing M_4AlC_3 MAX phases using XRD and gaining insight into its potential Mo:Nb ordering by measuring their *c*-LPs, we focused on identifying the layered structure of MAX. To do so, we mapped Mo and Nb content using (scanning) transmission electron microscopy (S/TEM) with energy dispersive x-ray spectroscopy (EDS) and confirmed their expected coordination states using x-ray photoelectron spectroscopy (XPS). As shown in Figure S2, cross-sectional TEM revealed clear atomic layering of a grain of M_4AlC_3 MAX phase.[20] In addition, XPS corroborates that Mo, Nb, Al, and C exist in coordination states consistent with a M_4AlC_3 MAX phase, as shown in Figure S3. Finally, EDS confirmed the presence of Mo and Nb in the identified grains of M_4AlC_3 MAX phases (Figure 2d). Interestingly, we noted visually that the content of Mo and Nb change depending on which composition of MAX phase was observed. This mapping combined with M_4AlC_3 XRD patterns for Mo:Nb 2:2 to 2.7:1.3 ratios (Figure 2b) with only slight peak shifts (Figure 2c) indicated that the structure can possibly be an ordered phase in agreement with previous DFT predictions.[10, 14] However, we believed there was a slight intermixing behavior of Mo and Nb atoms (in Mo > 2) due to the small *c*-LP and EDS mapping changes.

To begin to characterize the Mo and Nb occupancies in the M_4AlC_3 MAX phase, we classified Mo:Nb ordering possibilities into three groups (Figure 3a). These are identified as fully ordered $Mo_2Nb_2AlC_3$, where Mo atoms occupy only the outer two M layers (M') and Nb atoms occupy only the inner two M layers (M") of M_4C_3 similar to Mo and Ti in $Mo_2Ti_2AlC_3$;[18] ordered $Mo_{2+\alpha}Nb_{2-\alpha}AlC_3$, where Mo and Nb preferentially occupy M atomic layers with some Mo-Nb intermixing in the layers; and fully disordered $(Mo_{1-y}Nb_y)_4AlC_3$, where a random solid solution of Mo and Nb occupy the M atomic layers similar to $(Mo_{1-y}V_y)_4AlC_3$.[11]

Figure 3. Characterization of Mo and Nb occupancies in the M' and M" sites. (a) Schematic of ordering in the M_4AlC_3 structure, showing order or disorder of Mo and Nb in the M' and M" sites, respectively. (b) Effect of Mo and Nb ordering on the formation energy of a M_4AlC_3 structure. (c) Energy difference between changing Mo and Nb occupancies off of a perfect $Mo_2Nb_2AlC_3$ structure with Mo and Nb in the M' and M" sites, respectively. (d) Content of M_4AlC_3 compared to impurities as determined using the XRD data. (e) Occupancy of Mo and Nb in the M' and M" sites as determined by Rietveld refinement of the XRD data. (f) Molar content of Mo and Nb in the MAX structure as measured by EDS and XRD/Rietveld refinement.

To understand the occupancy preference of Mo and Nb in the distinct M atomic planes, we characterized the structure and energetics of the MAX phase as a function of Mo:Nb ratio and layer ordering using DFT. We used the Perdew-Burke-Ernzerhof (PBE) exchange-correlation functional and projector-augmented wave (PAW) pseudopotentials in the Vienna Ab initio Simulation Package (VASP).[21-24] See SI for computational details. In our simulations, we varied the Mo:Nb molar content between 2:2 and 3.2:0.8 and the fraction of Mo-Nb intermixing between the M' and M" layers to allow for direct comparison with experimental results.

Figure 3b shows the formation energy per formula unit (M_4AlC_3) as a function of composition for various degrees of Mo-Nb intermixing from no Nb in M' (0 at% substitutional fraction, dark green color) to all Nb in the M' layer (100 at% substitutional fraction, red color). We note that all of the explored systems in this figure are Mo-rich (Mo > 2 moles), and the atomic percent (at%) here presents the at% of the starting molar ratio of Nb atoms substituted in the M' layer and not the at% of the M' layer sites. Figure 3b highlights that M_4AlC_3 structures using Mo:Nb:Al:C mixtures with Mo preferentially occupying the outer M' layers and Nb the middle M" layers are energetically favorable as compared to competing phases. Figure 3c shows the energy difference

between the structures with no Nb substitution on M' layers (0 at%) and those with various degrees of substitution. We find that generally Nb substitution in the M' layers is typically less stable as compared to no Nb in the M' layers (Fig. 3c). In addition, we can see that the energetic driving force towards ordering of Mo and Nb decreases with increasing Mo content, understood by the stoichiometrically necessary interlayer mixing in the M" layer of the Mo-rich materials.

Next, we used XRD to analyze the range of mixed powders which result in more phase-pure M_4AlC_3 systems (Figure 3d). We chose this tool of analysis as completely solid solution MAX phases, such as $(Mo_{1-\gamma}V_\gamma)_4AlC_3$, tend to yield high-purity MAX phases in a wide range of possible transition metal mixtures.[9, 11] However, our results indicate that only Mo:Nb:Al:C combinations of 2.0:2.0:1.1:2.7 to 2.7:1.3:1.1:2.7 had M_4AlC_3 phase contents above 85 wt%, which implies that Mo:Nb molar ratios outside of 2.0:2.0 to 2.7:1.3 lead to other competing phases and less than 30 wt% MAX phase content (Figure 3d). To analyze the intermixing of Mo and Nb in the M' and M" sites in the experimentally synthesized M_4AlC_3 systems, we used Rietveld refinement (Figure S4). Specifically, as shown in Figure 3e, the substitutional fraction of Nb in the Mo-dominant M' site and Mo in the Nb-dominant M" site ranges from 9.5 at% to 4.4 at% and 8.8 at% to 19.7 at%, respectively. Using this occupancy data in Figure 3e, we calculated the atomic composition of our M_4AlC_3 MAX phases to roughly corroborate compared to EDS in Figure 3f. Although we noted a similar trend in Mo:Nb content, direct comparison is difficult as EDS cannot determine contribution from underlying impurity phases.

Our Rietveld data shows that the M_4AlC_3 structure varies in Mo:Nb content from a $Mo_{2.03}Nb_{1.93}AlC_3$ structure to $Mo_{2.34}Nb_{1.66}AlC_3$ for Mo:Nb:Al:C powder mixtures of 2.2:1.8:1.1:2.7 to 3.2:0.8:1.1:2.7. This narrow (~0.3 mol) variation in Mo content in the M_4AlC_3 phase across all mixtures illustrates that ordering of Mo and Nb in M' and M", respectively, is the likely preference for the Mo:Nb system, as entirely disordered systems would not illustrate this small ~0.3 mol change in Mo content amongst a mixed powder ratio range from 2.0:2.0:1.1:2.7 to 3.2:0.8:1.1:2.7. Overall, these results suggest that the M_4AlC_3 MAX phase synthesized using Mo and Nb is an ordered $Mo_2Nb_2AlC_3$ MAX phase with the exact composition of $Mo_{2+\alpha}Nb_{2-\alpha}AlC_3$ ($0 \leq \alpha \leq 0.3$), which is a level of tunability in ordered double metal MAX phases has not been observed previously. However, further experimentation using more direct observation methods, such as a recent publication using secondary ion mass spectrometry,[25] which can avoid the small difference in valence electrons ($4d^2$ for Nb, $4d^3$ for Mo) is necessary to fully understand the ordering of Mo and Nb in the M' and M" sites.

Figure 4. Etching and delamination of the $Mo_{2+\alpha}Nb_{2-\alpha}AlC_3$ to yield $Mo_{2+\alpha}Nb_{2-\alpha}C_3T_x$ MXenes using an HF-TMAOH approach. (a) Generalized schematic representation of the etching, delamination, and free-standing film preparation of $Mo_{2+\alpha}Nb_{2-\alpha}C_3T_x$ films. (b) Full-pattern XRD of the $Mo_{2+\alpha}Nb_{2-\alpha}AlC_3$ MAX phase, etched $Mo_{2+\alpha}Nb_{2-\alpha}C_3T_x$ MXene powder, and free-standing $Mo_{2+\alpha}Nb_{2-\alpha}C_3T_x$ delaminated MXene film (actual composition derived from Rietveld in parenthesis). (c) Focus on the (002) peaks from the full-pattern XRD reveals the left-shift in the (002) peak of $Mo_{2+\alpha}Nb_{2-\alpha}AlC_3$ to yield $Mo_{2+\alpha}Nb_{2-\alpha}C_3T_x$ MXenes (actual composition derived from Rietveld in parenthesis). (d-f) SEM images of the $Mo_{2+\alpha}Nb_{2-\alpha}AlC_3$ MAX phase through to the $Mo_{2+\alpha}Nb_{2-\alpha}C_3T_x$ MXene free-standing film.

After determining the preferential occupancy of Mo and Nb in the M' and M" layers, in the $Mo_{2+\alpha}Nb_{2-\alpha}AlC_3$ MAX phase, we next looked to synthesize the resultant $Mo_{2+\alpha}Nb_{2-\alpha}C_3T_x$ o-

MXenes using a selective etching and delamination approach (Figure 4a). To identify the optimum etching condition, we first synthesized $Mo_{2+\alpha}Nb_{2-\alpha}C_3T_x$ o-MXenes using 50% hydrofluoric acid for 2 and 4 days at 55 °C. We noted that 4 days was necessary to produce $Mo_{2+\alpha}Nb_{2-\alpha}C_3T_x$ MXenes from their respective MAX phases, as the (002) peaks left-shift from ~7.6° 2θ to ~5.8° 2θ (Figures 4b-c and S5). This shift in (002) peak position indicates an interlayer expansion of ~3.6 Å, suggesting the removal of Al between the $Mo_{2+\alpha}Nb_{2-\alpha}C_3$ layers and intercalation of water molecules (Figures 4c and S5).[11] We can also see the change in the appearance from MAX to MXenes, as shown in Figure 4d-e.[26] Although the data shown in Figure 4b-f is for the MAX synthesized using a Mo:Nb ratio of 2.7:1.3, all $Mo_{2+\alpha}Nb_{2-\alpha}C_3T_x$ MXenes are shown in Figure S5. We also used a milder etchant by using a mixture of 5% HF and 7.2 M HCl at 55 °C for 4 days (referred to as HF/HCl) to yield $Mo_{2+\alpha}Nb_{2-\alpha}C_3T_x$ MXenes. A partial shift of the (002) peak from ~7.6° 2θ to ~5.9° 2θ was observed, indicating an interlayer expansion of 3.3 Å, but was insufficient to completely etch Al layers away from the MAX phases (Figure S6).

After successfully exfoliating the Al layers in the MAX phases to yield MXenes, we used two methods to delaminate the $Mo_{2+\alpha}Nb_{2-\alpha}C_3T_x$ multilayer powders into single-to-few layer flakes, made by 50% HF (referred to as HF) and HF/HCl. For the HF-etched $Mo_{2+\alpha}Nb_{2-\alpha}C_3T_x$, we utilized 5 wt% tetramethylammonium hydroxide (TMAOH) to delaminate the MXene, similar to previous reports (HF-TMAOH approach).[26] For the $Mo_{2+\alpha}Nb_{2-\alpha}C_3T_x$ produced using the HF/HCl approach, we utilized 0.5 M LiCl as the delamination agent.[27, 28] For the HF-TMAOH $Mo_{2+\alpha}Nb_{2-\alpha}C_3T_x$ MXene, we were able to obtain free-standing single-to-few layer MXene flakes (Figure S7) and vacuum filtrated the colloidal solution to make free-standing films (cross-section in Figure 4f). The XRD of this film showed a shift in (002) peak position to ~5.1° 2θ (Figures 4c and S8) which indicates an interlayer expansion of 5.7 Å total from the original MAX phase, which is consistent with other $M_4C_3T_x$ MXenes.[11] Although LiCl delaminated HF-HCl etched $Mo_{2+\alpha}Nb_{2-\alpha}C_3T_x$ produced single-to-few layer flakes (Figure S9), the yield was not enough to produce free-standing films (yields in Table S3).

The etching and delamination conditions can affect the MXene flake morphology.[8, 29] When comparing the HF-TMAOH produced (Figure S7) and HF/HCl-LiCl produced (Figure S9) single-flakes of $Mo_{2+\alpha}Nb_{2-\alpha}C_3T_x$, we note that HF-TMAOH produced $Mo_{2+\alpha}Nb_{2-\alpha}C_3T_x$ are plentiful in single-to-few monolayer forms while HF/HCl-LiCl produced $Mo_{2+\alpha}Nb_{2-\alpha}C_3T_x$ are single-to-few flakes with some multilayer-flakes. Although the HF-TMAOH produced flakes have more single-to-few layer flakes, it is also known that HF-TMAOH MXenes have TMA^+ cations on their surfaces which prevents their attachment to electrodes, as seen in Figure S10. As a result of this attachment issue, we focused on characterizing HF/HCl-LiCl produced $Mo_{2+\alpha}Nb_{2-\alpha}C_3T_x$ MXene for their HER capability.

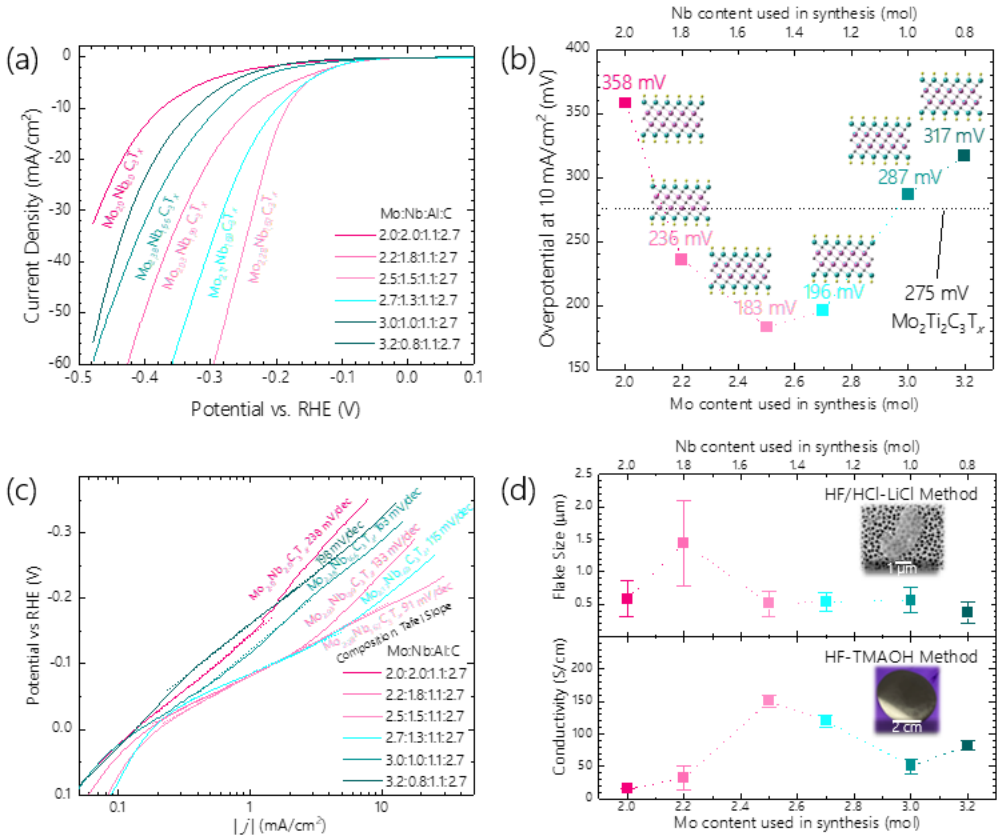

Figure 5. Hydrogen evolution reaction (HER) characterization of HF/HCl-LiCl produced $Mo_{2+\alpha}Nb_{2-\alpha}C_3T_x$ MXenes. (a) Potential vs. current density plots of $Mo_{2+\alpha}Nb_{2-\alpha}C_3T_x$ MXenes (Mo:Nb:Al:C composition in legend, actual Rietveld-derived composition next to data)used to derive overpotentials at -10 mA/cm^2 and tafel slopes shown in panels (b) and (c), respectively. (d) Conductivity measurements of HF-TMAOH synthesized $Mo_{2+\alpha}Nb_{2-\alpha}C_3T_x$ MXenes compared to flake sizes of HF-HCl/LiCl synthesized $Mo_{2+\alpha}Nb_{2-\alpha}C_3T_x$ MXenes.

To begin our catalysis experiments, we drop casted HF-HCl/LiCl synthesized single-to-few layer $Mo_{2+\alpha}Nb_{2-\alpha}C_3T_x$ MXenes onto glassy carbon electrodes and used a three-electrode electrochemical cell. Details found in the SI. In the resultant linear sweep voltammograms (LSVs), we noted $Mo_{2+\alpha}Nb_{2-\alpha}C_3T_x$ MXenes produced using Mo:Nb ratios of 2.2:1.8 to 2.7:1.3, as shown in Figure 5a, were found to own improved HER performance as compared to other $Mo_{2+\alpha}Nb_{2-\alpha}C_3T_x$ MXenes and $Mo_2Ti_2C_3T_x$ produced using the same method. A similar plot showing the poor HER catalytic behavior of HF-TMAOH produced $Mo_{2+\alpha}Nb_{2-\alpha}C_3T_x$ MXene is also shown in Figure S11.

In Figure 5b we present the overpotential of each $Mo_{2+\alpha}Nb_{2-\alpha}C_3T_x$ MXene at a current density of -10 mA/cm^2. To compare these overpotentials of HF/HCl-LiCl $Mo_{2+\alpha}Nb_{2-\alpha}C_3T_x$ MXenes to another $M_4C_3T_x$ MXene containing Mo in the M' site, we synthesized and conducted HER characterization on single-to-few layer flakes of $Mo_2Ti_2C_3T_x$ (Figure S12), which its HER was reported previously [30] When we compared the overpotentials of $Mo_{2+\alpha}Nb_{2-\alpha}C_3T_x$ MXenes to $Mo_2Ti_2C_3T_x$ (275 mV), we noted that $Mo_{2+\alpha}Nb_{2-\alpha}C_3T_x$ MXenes synthesized from MAX phases with Mo:Nb mixtures from 2.2:1.8 to 2.7:1.3 outperformed $Mo_2Ti_2C_3T_x$ as shown in Figure 5b. As shown in Figure 5c, Tafel slopes derived from the potential vs. current density plots shown in

Figure 5a illustrate that $Mo_{2+\alpha}Nb_{2-\alpha}C_3T_x$ MXene synthesized using a Mo:Nb ratios of 2.5:1.5 and 2.7:1.3 continues to outperform as compared to other $Mo_{2+\alpha}Nb_{2-\alpha}C_3T_x$ MXenes with a slope of 91 mV/dec and 115 mV/dec, respectively. This performance is not likely an effect of larger flakes with more exposed basal plane,[30] as the average flake size for HF/HCl-LiCl synthesized MXenes is lower for that of 2.5:1.5 and 2.7:1.3 as compared to 2:2 or 2.2:1.8 (Figure 5d). Overall, although this performance does not yet approach the HER performance of previously reported Pt/C catalysts, MXenes' inherent solution processability and earth-abundance of the precursor transition metals and carbon illustrates $Mo_{2+\alpha}Nb_{2-\alpha}C_3T_x$ MXenes' potential for cost-effective use in HER applications.[31-34]

Therefore, this outperformance of Mo:Nb 2.5:1.5 and 2.7:1.3 may be partially linked to the occupancies of Mo and Nb in the M' and M'' sites. As we presented in in Figure 3e, the phases with Mo:Nb as 2.5:1.5 and 2.7:1.3 have the formula of $Mo_{2.28}Nb_{1.67}C_3T_x$ and $Mo_{2.17}Nb_{1.69}C_3T_x$ which indicate comparatively higher concentrations of Mo in the M'' site at 19.7 at% and 14.2 at%, respectively. Another contributing factor can be the change in electronic properties and the resulting electrical conductivity of MXenes because of the Mo:Nb occupancies. Due to the poor yield of HF/HCl-LiCl synthesized $Mo_{2+\alpha}Nb_{2-\alpha}C_3T_x$ MXenes (Table S3), we focused on measuring the electrical conductivity of HF-TMAOH synthesized $Mo_{2+\alpha}Nb_{2-\alpha}C_3T_x$ MXene films as shown in Figure 5d to demonstrate the effect of composition on the electrical conductivity of the HF-TMAOH produced flexible $Mo_{2+\alpha}Nb_{2-\alpha}C_3T_x$ MXenes films (Figure 5d) (image of film in Figure S13). Details of the electrical conductivity values can be found in Table S4.

The electrical conductivities of 150.5 S/cm and 120.0 S/cm of Mo:Nb 2.5:1.5 and 2.7:1.3, respectively, are the highest of all $Mo_{2+\alpha}Nb_{2-\alpha}C_3T_x$ MXenes and higher than $Mo_2Ti_2C_3T_x$ (55.8 S/cm) produced using the same method. This increase in electrical conductivity of $Mo_{2.28}Nb_{1.67}C_3T_x$ and $Mo_{2.17}Nb_{1.69}C_3T_x$ (original Mo:Nb mixture of 2.5:1.5 and 2.7:1.3, respectively) as compared to the other $Mo_{2+\alpha}Nb_{2-\alpha}C_3T_x$ MXenes indicate that there are likely some changes in the electronic properties as a result of Mo intermixing in the M' layer, which improves their HER behavior. [35] In addition, the lower electrical conductivity of HF-TMAOH produced $Mo_{2+\alpha}Nb_{2-\alpha}C_3T_x$ MXenes of Mo:Nb of 2.7:1.3 or higher as compared to Mo:Nb of 2.5:1.5 might be linked to the smaller flake sizes. Similarly, the HER behavior of Mo:Nb of 3.0:1.0 and higher can be attributed to more multi-layer flakes as seen in Figure S9. However, a fundamental understanding of the relation of M' and M'' site occupancies with relation of the electronic structure to the catalytic performance of o-MXenes is not yet fully understood.

Nevertheless, we next compared our $Mo_{2.28}Nb_{1.67}C_3T_x$ MXene HER catalytic behavior to other Mo-containing MXenes as shown in Figure S15, such as $Mo_2Ti_2C_3T_x$ (re-tested in this study), $Mo_{1.33}CT_x$,[36] and Mo_2CT_x MXenes [37] and found that $Mo_{2.28}Nb_{1.67}C_3T_x$ has an overpotential (183 mV) comparable to that of Mo_2CT_x MXene (~160 mV).[37] Although it is important to note that Mo_2CT_x was synthesized with a different approach, this data implies that Mo-containing $M_4C_3T_x$ MXenes can approach HER catalysis values reported for Mo-containing M_2CT_x MXenes. Development of $M_4C_3T_x$ with comparatively low overpotentials is potentially significant for MXene catalysts, as MXenes with a higher n in the $M_{n+1}X_nT_x$ structure have shown improved performances in degrading environments,[38, 39] although future studies are highly necessary to elucidate this point.

In summary, we have reported an ordered $Mo_{2+\alpha}Nb_{2-\alpha}AlC_3$ MAX phase ($0 \leq \alpha \leq 0.3$) and characterized its composition and partial ordering in-depth using a combination of XRD, XPS, TEM, EDS, Rietveld, and DFT methods. We have also characterized these derivative $Mo_{2+\alpha}Nb_{2-\alpha}C_3T_x$ o-MXenes for their HER catalytic potential and identified the low overpotential (183 mV) for the $Mo_{2.28}Nb_{1.67}C_3T_x$ MXene. This study further expands the possible compositional control of ordered double-transition metal MXenes toward the application-driven design of 2D materials.

Supporting Information:

Experimental methods, XRD of all attempted compositions of Mo:Nb:Al:C, TEM of the MAX phase cross section, lattice constants of the synthesized $Mo_{2+\alpha}Nb_{2-\alpha}$ AlC_3 MAX, XPS of synthesized $Mo_{2+\alpha}Nb_{2-\alpha}$ AlC_3 structures with deconvolution details, Rietveld Refinements plots with fitting, XRD of various etching procedures described in the main text, SEM of single-to-few layer flakes of $Mo_{2+\alpha}Nb_{2-\alpha}$ C_3T_x MXenes synthesized by both HF-TMAOH and HF/HCl-LiCL approaches, XRD of free-standing single-to-few layer flakes of $Mo_{2+\alpha}Nb_{2-\alpha}$ C_3T_x MXene films, yields of single-to-few layer flakes of $Mo_{2+\alpha}Nb_{2-\alpha}$ C_3T_x MXenes produced using HF-TMAOH and HF/HCl-LiCl methods, HER plots of HF-TMAOH synthesized single-to-few layer flakes of $Mo_{2+\alpha}Nb_{2-\alpha}$ C_3T_x MXenes and $Mo_2Ti_2C_3T_x$ MXenes, flake sizes of HF-TMAOH produced single-to-few layer flakes of $Mo_{2+\alpha}Nb_{2-\alpha}$ C_3T_x MXenes, digital image of a free-standing $Mo_{2+\alpha}Nb_{2-\alpha}$ C_3T_x MXene film, and comparative plot of single-to-few layer flakes of $Mo_{2+\alpha}Nb_{2-\alpha}$ C_3T_x MXene to other Mo-containing MXenes.

Acknowledgements:

We acknowledge the support from US National Science Foundation under grant numbers DMR-SSMC 2124478 and 2124241. Computational resources from nanoHUB and Purdue University are gratefully acknowledged. B.C.W. acknowledges financial support from the National Defense Engineering & Science Graduate Fellowship Program.

Competing interests:

The authors claim no competing financial interests.

TOC:

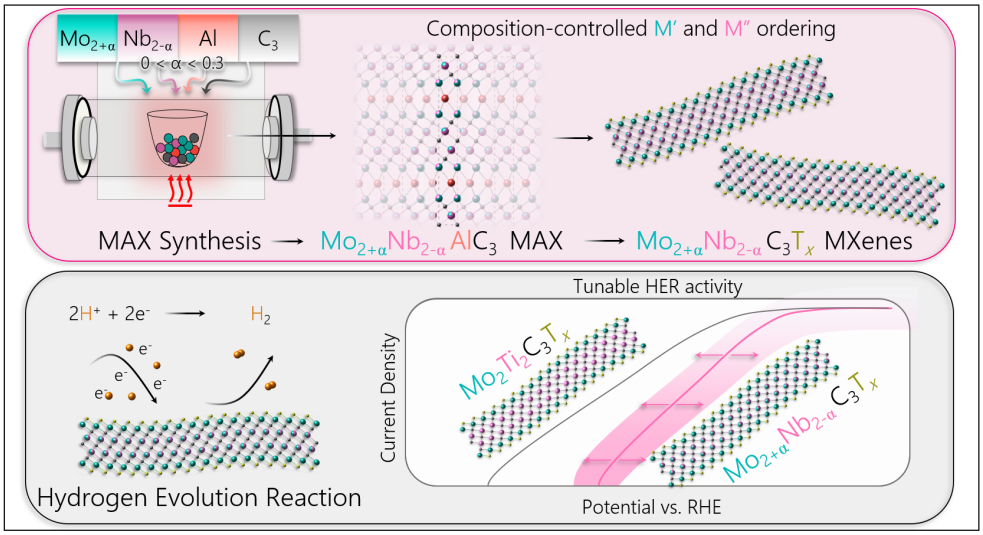
Mo2+α
Nb2-α
Al
C3
0 < α < 0.3
Composition-controlled M′ and M″ ordering
MAX Synthesis
Mo2+αNb2-αAlC3 MAX
Mo2+αNb2-αC3Tx MXenes
2H+ + 2e-
H2
e-
Hydrogen Evolution Reaction
Tunable HER activity
Current Density
Mo2Ti2C3Tx
C3Tx
Mo2+αNb2-α
Potential vs. RHE

References

(1) Bonaccorso, F.; Colombo, L.; Yu, G.; Stoller, M.; Tozzini, V.; Ferrari, A. C.; Ruoff, R. S.; Pellegrini, V. 2D materials. Graphene, related two-dimensional crystals, and hybrid systems for energy conversion and storage. *Science* **2015**, *347* (6217), 1246501. DOI: 10.1126/science.1246501.

(2) Pomerantseva, E.; Gogotsi, Y. Two-dimensional heterostructures for energy storage. *Nature Energy* **2017**, *2* (7). DOI: 10.1038/nenergy.2017.89.

(3) Lukatskaya, M. R.; Kota, S.; Lin, Z.; Zhao, M.-Q.; Shpigel, N.; Levi, M. D.; Halim, J.; Taberna, P.-L.; Barsoum, M. W.; Simon, P.; et al. Ultra-high-rate pseudocapacitive energy storage in two-dimensional transition metal carbides. *Nature Energy* **2017**, *2* (8). DOI: 10.1038/nenergy.2017.105.

(4) Wu, W.; Wang, L.; Li, Y.; Zhang, F.; Lin, L.; Niu, S.; Chenet, D.; Zhang, X.; Hao, Y.; Heinz, T. F.; et al. Piezoelectricity of single-atomic-layer MoS2 for energy conversion and piezotronics. *Nature* **2014**, *514* (7523), 470-474. DOI: 10.1038/nature13792.

(5) Peng, L.; Xiong, P.; Ma, L.; Yuan, Y.; Zhu, Y.; Chen, D.; Luo, X.; Lu, J.; Amine, K.; Yu, G. Holey two-dimensional transition metal oxide nanosheets for efficient energy storage. *Nat Commun* **2017**, *8*, 15139. DOI: 10.1038/ncomms15139.

(6) Naguib, M.; Barsoum, M. W.; Gogotsi, Y. Ten Years of Progress in the Synthesis and Development of MXenes. *Adv Mater* **2021**, *33* (39), e2103393. DOI: 10.1002/adma.202103393.

(7) Gogotsi, Y.; Anasori, B. The Rise of MXenes. *ACS Nano* **2019**, *13* (8), 8491-8494. DOI: 10.1021/acsnano.9b06394.

(8) Lim, K. R. G.; Shekhirev, M.; Wyatt, B. C.; Anasori, B.; Gogotsi, Y.; Seh, Z. W. Fundamentals of MXene synthesis. *Nature Synthesis* **2022**. DOI: 10.1038/s44160-022-00104-6.

(9) Hong, W.; Wyatt, B. C.; Nemani, S. K.; Anasori, B. Double transition-metal MXenes: Atomistic design of two-dimensional carbides and nitrides. *MRS Bulletin* **2020**, *45* (10), 850-861. DOI: 10.1557/mrs.2020.251.

(10) Anasori, B.; Xie, Y.; Beidaghi, M.; Lu, J.; Hosler, B. C.; Hultman, L.; Kent, P. R.; Gogotsi, Y.; Barsoum, M. W. Two-Dimensional, Ordered, Double Transition Metals Carbides (MXenes). *ACS Nano* **2015**, *9*, 9507-9516.

(11) Pinto, D.; Anasori, B.; Avireddy, H.; Shuck, C. E.; Hantanasirisakul, K.; Deysher, G.; Morante, J. R.; Porzio, W.; Alshareef, H. N.; Gogotsi, Y. Synthesis and electrochemical properties of 2D molybdenum vanadium carbides – solid solution MXenes. *Journal of Materials Chemistry A* **2020**, *8* (18), 8957-8968. DOI: 10.1039/d0ta01798a.

(12) Han, M.; Shuck, C. E.; Rakhmanov, R.; Parchment, D.; Anasori, B.; Koo, C. M.; Friedman, G.; Gogotsi, Y. Beyond $Ti_3C_2T_x$: MXenes for Electromagnetic Interference Shielding. *ACS Nano* **2020**, *14* (4), 5008-5016. DOI: 10.1021/acsnano.0c01312.

(13) Meshkian, R.; Tao, Q.; Dahlqvist, M.; Lu, J.; Hultman, L.; Rosen, J. Theoretical stability and materials synthesis of a chemically ordered MAX phase, Mo_2ScAlC_2, and its two-dimensional derivate Mo_2ScC_2 MXene. *Acta Materialia* **2017**, *125*, 476-480. DOI: 10.1016/j.actamat.2016.12.008.

(14) Dahlqvist, M.; Rosen, J. Predictive theoretical screening of phase stability for chemical order and disorder in quaternary 312 and 413 MAX phases. *Nanoscale* **2020**, *12* (2), 785-794. DOI: 10.1039/c9nr08675g.

(15) Caspi, E. a. N.; Chartier, P.; Porcher, F.; Damay, F.; Cabioc'h, T. Ordering of (Cr, V) layers in nanolamellar $(Cr_{0.5}V_{0.5})_{n+1}AlC_n$ compounds. *Materials Research Letters* **2015**, *3* (2), 100-106.

(16) Tunca, B.; Lapauw, T.; Karakulina, O. M.; Batuk, M.; Cabioc'h, T.; Hadermann, J.; Delville, R.; Lambrinou, K.; Vleugels, J. Synthesis of MAX Phases in the Zr-Ti-Al-C System. *Inorg Chem* **2017**, *56* (6), 3489-3498. DOI: 10.1021/acs.inorgchem.6b03057.
(17) Shuck, C. E.; Han, M.; Maleski, K.; Hantanasirisakul, K.; Kim, S. J.; Choi, J.; Reil, W. E. B.; Gogotsi, Y. Effect of Ti_3AlC_2 MAX Phase on Structure and Properties of Resultant $Ti_3C_2T_x$ MXene. *ACS Applied Nano Materials* **2019**, *2* (6), 3368-3376. DOI: 10.1021/acsanm.9b00286.
(18) Anasori, B.; Dahlqvist, M.; Halim, J.; Moon, E. J.; Lu, J.; Hosler, B. C.; Caspi, E. a. N.; May, S. J.; Hultman, L.; Eklund, P.; et al. Experimental and theoretical characterization of ordered MAX phases Mo_2TiAlC_2 and $Mo_2Ti_2AlC_3$. *Journal of Applied Physics* **2015**, *118* (9). DOI: 10.1063/1.4929640.
(19) Pyykko, P.; Atsumi, M. Molecular single-bond covalent radii for elements 1-118. *Chemistry* **2009**, *15* (1), 186-197. DOI: 10.1002/chem.200800987.
(20) Rigby-Bell, M. T. P.; Natu, V.; Sokol, M.; Kelly, D. J.; Hopkinson, D. G.; Zou, Y.; Bird, J. R. T.; Evitts, L. J.; Smith, M.; Race, C. P.; et al. Synthesis of new M-layer solid-solution 312 MAX phases (Ta1−xTix)3AlC2 (x = 0.4, 0.62, 0.75, 0.91 or 0.95), and their corresponding MXenes. *RSC Advances* **2021**, *11* (5), 3110-3114. DOI: 10.1039/d0ra09761f.
(21) Blöchl, P. E.; Jepsen, O.; Andersen, O. K. Improved tetrahedron method for Brillouin-zone integrations. *Physical Review B* **1994**, *49* (23), 16223.
(22) Kresse, G.; Furthmüller, J. Efficiency of ab-initio total energy calculations for metals and semiconductors using a plane-wave basis set. *Computational materials science* **1996**, *6* (1), 15-50.
(23) Perdew, J. P.; Burke, K.; Ernzerhof, M. Generalized gradient approximation made simple. *Physical review letters* **1996**, *77* (18), 3865.
(24) Botana, A. S.; Norman, M. R. Electronic structure and magnetism of transition metal dihalides: bulk to monolayer. *Physical Review Materials* **2019**, *3* (4), 044001.
(25) Michałowski, P. P.; Anayee, M.; Mathis, T. S.; Kozdra, S.; Wójcik, A.; Hantanasirisakul, K.; Jóźwik, I.; Piątkowska, A.; Możdżonek, M.; Malinowska, A.; et al. Oxycarbide MXenes and MAX phases identification using monoatomic layer-by-layer analysis with ultralow-energy secondary-ion mass spectrometry. *Nature Nanotechnology* **2022**. DOI: 10.1038/s41565-022-01214-0.
(26) Nemani, S. K.; Zhang, B.; Wyatt, B. C.; Hood, Z. D.; Manna, S.; Khaledialidusti, R.; Hong, W.; Sternberg, M. G.; Sankaranarayanan, S. K. R. S.; Anasori, B. High-Entropy 2D Carbide MXenes: $TiVNbMoC_3$ and $TiVCrMoC_3$. *ACS Nano* **2021**, *15* (8), 12815-12825. DOI: 10.1021/acsnano.1c02775.
(27) Matthews, K.; Zhang, T.; Shuck, C. E.; VahidMohammadi, A.; Gogotsi, Y. Guidelines for Synthesis and Processing of Chemically Stable Two-Dimensional V_2CT_x MXene. *Chemistry of Materials* **2021**, *34* (2), 499-509. DOI: 10.1021/acs.chemmater.1c03508.
(28) Wyatt, B. C., Nemani, S.K., Desai, K., Kaur, H., Zhang, B., Anasori, B. High-Temperature Stability and Phase Transformations of Titanium Carbide ($Ti_3C_2T_x$) MXene. *Journal of Physics: Condensed Matter* **2021**, *33*. DOI: 10.1088/1361-648X/abe793.
(29) Shekhirev, M.; Busa, J.; Shuck, C. E.; Torres, A.; Bagheri, S.; Sinitskii, A.; Gogotsi, Y. Ultralarge Flakes of $Ti_3C_2T_x$ MXene via Soft Delamination. *ACS Nano* **2022**, *16* (9), 13695-13703.
(30) Handoko, A. D.; Fredrickson, K. D.; Anasori, B.; Convey, K. W.; Johnson, L. R.; Gogotsi, Y.; Vojvodic, A.; Seh, Z. W. Tuning the basal plane functionalization of two-dimensional metal carbides (MXenes) to control hydrogen evolution activity. *ACS Applied Energy Materials* **2017**, *1* (1), 173-180.
(31) Lim, K. R. G.; Handoko, A. D.; Nemani, S. K.; Wyatt, B.; Jiang, H. Y.; Tang, J.; Anasori, B.; Seh, Z. W. Rational Design of Two-Dimensional Transition Metal Carbide/Nitride (MXene)

Hybrids and Nanocomposites for Catalytic Energy Storage and Conversion. *ACS Nano* **2020**, *14* (9), 10834-10864. DOI: 10.1021/acsnano.0c05482.
(32) Chen, Z.; Wu, R.; Liu, Y.; Ha, Y.; Guo, Y.; Sun, D.; Liu, M.; Fang, F. Ultrafine Co nanoparticles encapsulated in carbon-nanotubes-grafted graphene sheets as advanced electrocatalysts for the hydrogen evolution reaction. *Advanced Materials* **2018**, *30* (30), 1802011.
(33) Zheng, Z.; Yu, L.; Gao, M.; Chen, X.; Zhou, W.; Ma, C.; Wu, L.; Zhu, J.; Meng, X.; Hu, J. Boosting hydrogen evolution on MoS2 via co-confining selenium in surface and cobalt in inner layer. *Nature communications* **2020**, *11* (1), 1-10.
(34) Zhong, Y.; Xia, X.; Shi, F.; Zhan, J.; Tu, J.; Fan, H. J. Transition metal carbides and nitrides in energy storage and conversion. *Advanced science* **2016**, *3* (5), 1500286.
(35) Pan, H. Ultra-high electrochemical catalytic activity of MXenes. *Scientific reports* **2016**, *6* (1), 1-10.
(36) Meshkian, R.; Dahlqvist, M.; Lu, J.; Wickman, B.; Halim, J.; Thornberg, J.; Tao, Q.; Li, S.; Intikhab, S.; Snyder, J.; et al. W-Based Atomic Laminates and Their 2D Derivative $W_{1.33}C$ MXene with Vacancy Ordering. *Adv Mater* **2018**, *30* (21), e1706409. DOI: 10.1002/adma.201706409.
(37) Lim, K. R. G.; Handoko, A. D.; Johnson, L. R.; Meng, X.; Lin, M.; Subramanian, G. S.; Anasori, B.; Gogotsi, Y.; Vojvodic, A.; Seh, Z. W. 2H-MoS_2 on Mo_2CT_x MXene Nanohybrid for Efficient and Durable Electrocatalytic Hydrogen Evolution. *ACS Nano* **2020**, *14* (11), 16140-16155. DOI: 10.1021/acsnano.0c08671.
(38) Huang, S.; Mochalin, V. N. Combination of High pH and an Antioxidant Improves Chemical Stability of Two-Dimensional Transition-Metal Carbides and Carbonitrides (MXenes) in Aqueous Colloidal Solutions. *Inorganic Chemistry* **2022**, *61* (26), 9877-9887.
(39) Wyatt, B. C., Rosenkranz, A., Anasori, B. 2D MXenes: Tunable Mechanical and Tribological Properties. *Advanced Materials* **2021**, *33* (6), 2007973. DOI: 10.1002/adma.202007973.